The Astrophysical Journal, 836:59 (8pp), 2017 February 10 https://doi.org/10.3847/1538-4357/836/1/59

Class II 6.7 GHz Methanol Maser Association with Young Massive Cores Revealed by ALMA

James O. Chibueze[1,2,3,8], Timea Csengeri[4], Ken'ichi Tatematsu[2,5], Tetsuo Hasegawa[2], Satoru Iguchi[2,5], Jibrin A. Alhassan[1], Aya E. Higuchi[6], Sylvain Bontemps[7], and Karl M. Menten[4]

[1] Department of Physics and Astronomy, Faculty of Physical Sciences, University of Nigeria, Carver Building, 1 University Road, Nsukka, Nigeria; james.chibueze@unn.edu.ng, jchibueze@ska.ac.za

[2] National Astronomical Observatory of Japan, National Institutes of Natural Sciences, 2-21-1 Osawa, Mitaka, Tokyo 181-8588, Japan

[3] SKA Africa, 3rd Floor, The Park, Park Road, Pinelands, Cape Town, 7405, South Africa

[4] Max Planck Institute for Radioastronomy, Auf dem Hügel 69, D-53121 Bonn, Germany

[5] Department of Astronomical Science, SOKENDAI (The Graduate University for Advanced Studies), 2-21-1 Osawa, Mitaka, Tokyo 181-8588, Japan

[6] The Institute of Physical and Chemical Research (RIKEN), 2-1, Hirosawa, Wako-shi, Saitama 351-0198, Japan

[7] OASU/LAB-UMR5804, CNRS, Université Bordeaux 1, F-33270 Floirac, France

[8] Space Research Unit, Physics Department, NorthWest University, Private Bag X6001, Potchefstroom, 2520, South Africa

Received 2016 November 25; revised 2017 January 10; accepted 2017 January 10; published 2017 February 8

Abstract

We explored the implication of the association (or lack of it) of 6.7 GHz class II methanol (CH_3OH) masers with massive dense cores (MDCs) detected (within a sample of ATLASGAL selected infrared quiet massive clumps) at 0.9 mm with Atacama Large Millimeter/submillimeter array. We found 42 out of the 112 cores (37.5%) detected with the Atacama Compact Array (ACA) to be associated with 6.7 GHz CH_3OH masers. The lowest mass core with CH_3OH maser association is $\sim 12\ M_\odot$. The angular offsets of the ACA cores from the 6.7 GHz CH_3OH maser peak positions range from 0$''$17 to 4$''$79, with a median value of 2$''$19. We found a weak correlation between the 0.9 mm continuum (MDCs) peak fluxes and the peak fluxes of their associated methanol multibeam (MMB) 6.7 GHz CH_3OH masers. About 90% of the cores associated with 6.7 GHz CH_3OH masers have masses of $>40\ M_\odot$. The CH_3OH maser containing cores are candidates for embedded high-mass protostellar objects in their earliest evolutionary stages. With our ACA 0.9 continuum data compared with the MMB 6.7 GHz CH_3OH maser survey, we have constrained the cores already housing massive protostars based on their association with the radiatively pumped 6.7 GHz CH_3OH masers.

Key words: H II regions – stars: formation – stars: massive – surveys

Supporting material: figure set

1. Introduction

The formation process of massive stars is still strongly debated. High-mass stars influence the evolution of their host galaxies and the interstellar matter, thus underscoring the importance of understanding how they form. In spite of their typically far distances, and complex environments, recent studies have unveiled more clues like the presence of rotating structures/disks (Sánchez-Monge et al. 2013; Higuchi et al. 2015; Ilee et al. 2016), diversity in the physical conditions (associated with maser spots or not), jet/outflow, rotating structure/disk, and envelope structures from source to source contain important clues on the evolutionary processes in massive star formation (Chibueze et al. 2012).

Menten (1991) classified methanol (CH_3OH) masers into classes I and II. The key difference between the two lies in their excitation mechanisms. While class I CH_3OH masers are excited by collisional processes, class II masers are radiatively excited (Cragg et al. 1992, 2005; Sobolev & Deguchi 1994). There is high probability of finding class I CH_3OH masers around outflow shock interfaces around protostellar objects (Plambeck & Menten 1990; Kalenskii et al. 2010; Ilee et al. 2016), while the class II CH_3OH masers (especially 6.7 GHz CH_3OH masers) are found close to the central massive cores, sometimes with rotating (disk) structures (De Buizer 2003; Minier et al. 2003; Xu et al. 2008; Bartkiewicz et al. 2009; Cyganowski et al. 2009; Breen et al. 2013; Ilee et al. 2016).

Chemical evolution and astrophysical masers have been combined in attempts to establish an evolutionary sequence of massive stars (Codella et al. 2004; Breen et al. 2010, 2011; Urquhart et al. 2013a, 2013b; Gerner et al. 2014; de Villiers et al. 2015). While masers, especially 6.7 GHz CH_3OH and $\sim$22 GHz H_2O masers, serve as signposts of star formation, their use as independent evolutionary clocks is still being debated. H_2O maser excitation has been thought to precede CH_3OH masers, which in turn precedes OH masers with some level of overlap in time (Reid 2007). Based on a statistical analysis, de Villiers et al. (2015) argued that the outflows are launched prior to the excitation of 6.7 GHz (class II) CH_3OH masers. Forty-four GHz class I CH_3OH masers are known to trace outflow shock interface (see Ilee et al. 2016, Figure 1). Matsumoto et al. (2014) suggested that 44 GHz class I CH_3OH masers trace an earlier evolutionary stage than 6.7 GHz class II methanol masers. This is consistent with the statistical survey of Bayandina et al. (2012) in which they studied 206 44 GHz class I CH_3OH-maser sources and found 72% (148 sources) to be associated with 6.7 GHz class II CH_3OH masers and 83% to be associated with H_2O masers. The presence of more class I CH_3OH masers, compared to other maser species, supports de Villiers et al.'s (2015) argument that outflow precedes 6.7 GHz class II CH_3OH maser excitation, although mass bias may exist.

Combining millimeter observations with maser information could hold the key to unlocking the evolutionary sequence of

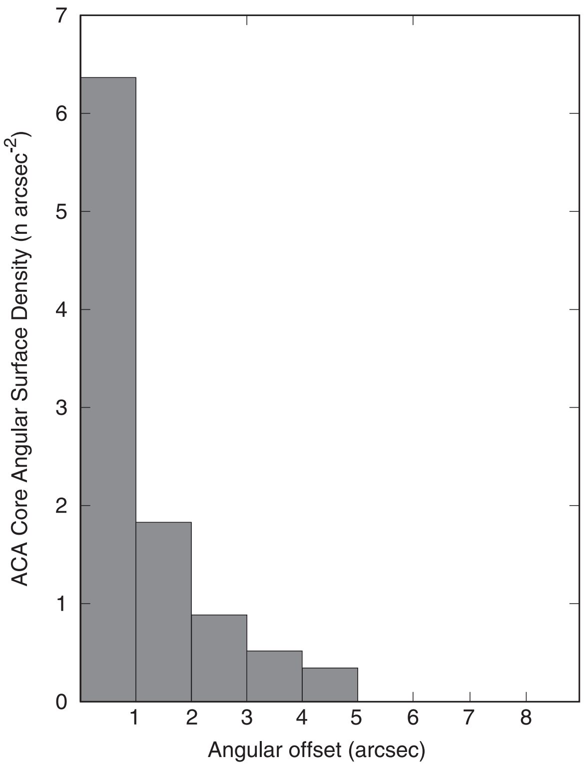

Figure 1. Angular surface density of MMB as a function positional separation between the MMB peak and ACA continuum core peaks.

high-mass stars. Masers serve as signposts of sites of active star formation (6.7 GHz CH_3OH masers exclusively associated with massive protostars). Toward a sample of young massive clumps selected from the 870 μm APEX Telescope LArge Survey of the GALaxy (ATLASGAL; Schuller et al. 2009; Contreras et al. (2013); Csengeri et al. 2014), Csengeri et al. (2017) presents the first Galaxy scale survey of massive cores with the Atacama Compact Array (ACA) reaching an angular resolution of 3″–5″, corresponding to 0.05–0.1 pc at a distance of $d < 5$ kpc. Details of the individual cores are discussed in Csengeri et al. (2017). The source selection criteria for the ALMA observations favor low bolometric luminosity ($L_{\rm bol} < 10^4\, L_\odot$) objects. In this paper, we statistically explore the association of masers (6.7 GHz class II CH_3OH masers), with massive cores/clumps detected with ALMA/ACA. Urquhart et al. (2013) presented a comparative study of ATLASGAL clumps associated with MMB 6.7 GHz CH_3OH masers; here we achieve nearly five times smaller angular resolution, which is needed to resolve the population of star-forming cores within massive clumps.

2. ALMA ACA Cores and Maser Catalogs

2.1. ALMA Data

The observations have been carried out in Cycle 2 with the ACA using 9–11 of the 7 m antennas. The lowest spectral resolution mode was used centered on 347.331, 345.796, 337.061, and 335.900 GHz, respectively, yielding 4×3.75 GHz effective bandwidth with a spectral resolution of 976.562 kHz. The primary beam size at this frequency is 28.″9. The details of the observing setup and data reduction procedure are described in Csengeri et al. (2017). Briefly, the data was calibrated using standard procedures in CASA 4.2.1. Line-free continuum images were obtained by excluding the channels with spectral lines toward each source, and then we averaged the remaining channels. For imaging, we used the CLEAN algorithm with a Brigg robust weight of 0.5 for the deconvolution. The synthesized size (geometric mean of the major and minor axes) beam varies between 3.″5 and 4.″6.

2.2. Maser Survey Data

We extracted the maser association information from catalogs of various maser species, which are summarized below. The 6.7 GHz CH_3OH masers were obtained from the methanol multibeam (MMB) catalog of Green et al. (2012; covering Galactic longitude 186°–330°), and Caswell et al. (2010, 2011; covering Galactic longitude 330°–6°).

The positional accuracy of the masers obtained with the Australia Telescope Compact Array (ATCA) is 0.″4 (this is better than the angular resolution of our ACA observations). We compared the positions of the MMB sources with that of the ALMA ACA sources from Csengeri et al. (2017). Maser sources within <5″ positional offset have been considered. The used survey covers 46–4 = 42 (91%) sources of the initial sample of Csengeri et al. (2017).

To check for the presence of 44 GHz class I CH_3OH masers, we have used the class I methanol maser catalog of Bayandina et al. (2012), which contains 206 sources selected from the literature up to the end of 2011 (see Bayandina et al. 2012 and references therein). Maser information extracted from individual publications lack completeness but we found 13% of the ALMA sources to be associated with 44 GHz class I CH_3OH masers, and in addition four with large offsets (>5″) from the ALMA cores.

The H_2O maser information was obtained from the H_2O Southern Galactic Plane Survey (HOPS) by Walsh et al. (2011). The positions of the H_2O maser emission reported by Walsh et al. (2011) are those of the brightest emission pixel in their data cube. This implies that weaker components of the H_2O masers, which may be associated with other cores. Also the positional accuracy of their survey is of the order of $\leqslant \sim 1'$. This suggests that H_2O masers are associated with the ALMA cores/clumps. We would like to note that the H_2O maser information of G351.4441+0.6579 [NGC 6334 I(N)] was taken from Chibueze et al. (2014).

3. Association and Selection Criteria

Our main focus is on the 6.7 GHz class II CH_3OH maser (MMB) association with the ACA cores (hereafter as ACA-MMB). The first selection condition is association with 6.7 GHz CH_3OH masers, and subsequently the selected cores were narrowed based on the following criteria:

(1) the distance to the core is <5 kpc (which has better reliability than the more distant source);
(2) the positional (angular) offset of the ACA core peak and the MMB peak is <5″.
(3) the difference between the $V_{\rm LSR}$ of the MMB peak and that of its associated ACA core (obtained from Csengeri et al. 2016) is within ± 8 km s^{-1}.

$>$Two ACA-MMB cores were *flagged*, i.e., dismissed from further consideration, because their peak flux densities were >1000 Jy (Fujisawa et al. 2014). This is to avoid contamination from possible maser flare incidents, as this will affect the

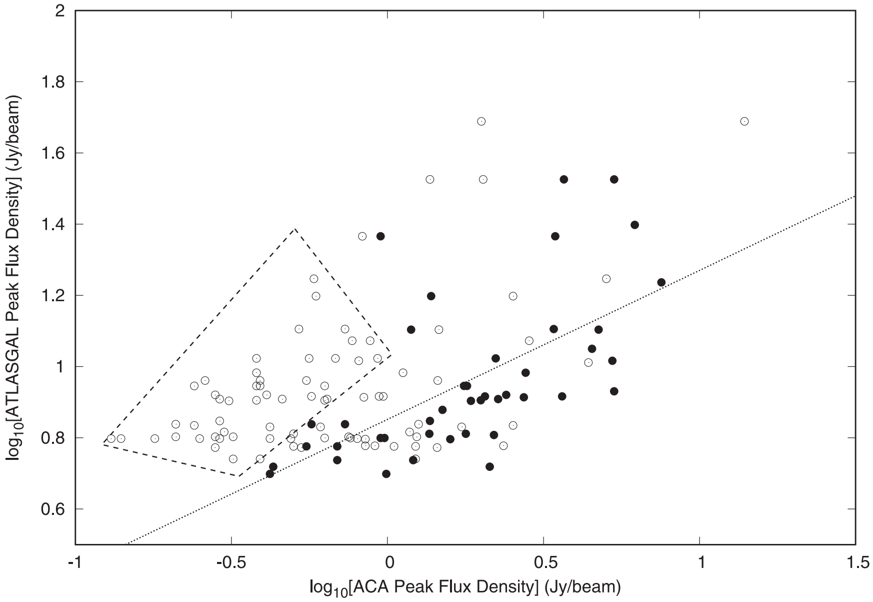

Figure 2. Plot of ATLASGAL clump peak flux densities against ACA core peak flux densities. Open circles represent sources without 6.7 GHz CH_3OH masers, while the filled circles are those associated with 6.7 GHz CH_3OH masers (*unflagged ACA-MMB*). The dotted line represents the best fit of the ATLASGAL-ACA flux relation of the 6.7 GHz CH_3OH maser-associated cores only. The skewed square represents the ACA weak-continuum region, which lacks CH_3OH maser emissions.

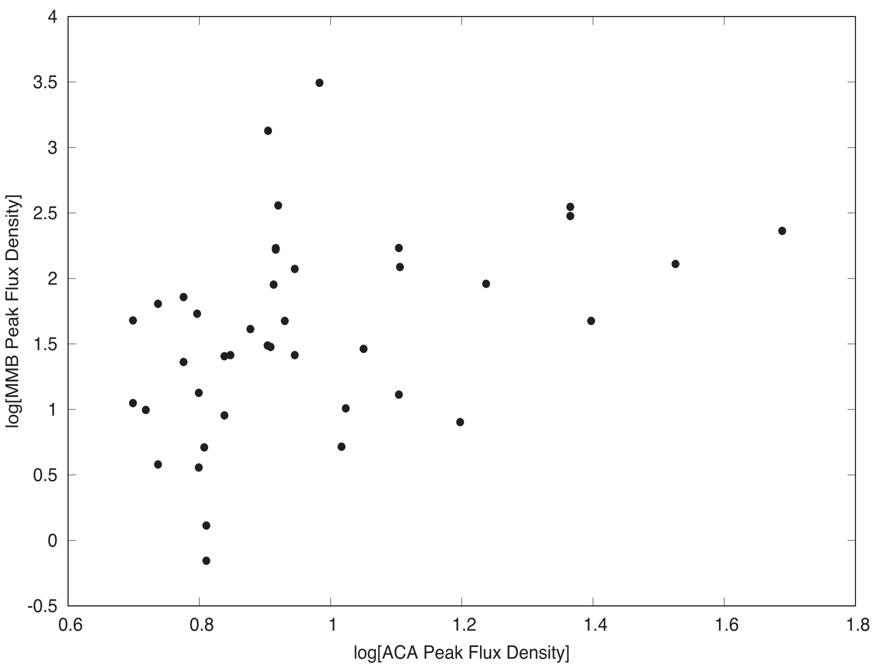

Figure 3. MMB-ACA peak flux densities.

comparative analyses done with the maser flux densities. We note that G335.5857−0.2906-MM1 has two distinct maser components but one ACA core peak. The maser component at V_{LSR} −47.3 km s^{-1} (the V_{LSR} of the core is −46.22 km s^{-1}) is spatially co-located with core peak (with 0″29 offset) while the second component at V_{LSR} −51.4 km s^{-1} is 3″18 offset from the core peak and could be associated with an unresolved core. We also have a similar situation in G348.5493−09789-MM1. 6.7 and 44 GHz CH_3OH masers of G351.7747−0.5369 are spatially coincident.

Because of lack of completeness within our sample, we have simply shown the positions of the 44/95 GHz class I CH_3OH masers and 22 GHz H_2O masers in the figures in the Appendix, but we did not use them for our statistical considerations and made no further discussions of them.

4. Results

Within the 46 ATLASGAL clumps observed with the ACA, a total of 125 cores were identified (see details in Csengeri et al. 2017). We have cross-matched the detected cores with the available maser catalogs (see Section 2.2). We could not confirm any previous CH_3OH maser observations toward 13 cores (associated with 4 clumps at decl. > 1°) out of the 125 detected with ACA, thus leaving us with a total of 112 ACA cores associated with 42 ATLASGAL clumps. On clump scale, 31 of the 42 (73.8%) clumps were associated with one of more

Table 1
Details of ACA Cores Associated with MMB 6.7 GHz CH_3OH Masers

Source Name	R.A. (deg)	Decl. (deg)	V_{LSR} (km s^{-1})	S_{peak} (Jy $beam^{-1}$)	Mass ($M_{\odot}$)	D_{kin} (kpc)	ACA-MMB Offset ($''$)	MMB S_{peak} (Jy $beam^{-1}$)	MMB V_{LSR} (km s^{-1})	MMB V_{range} (km s^{-1})
G320.2325−0.2844−MM1	227.4664	−58.4259	−66.30	1.59	147.80	3.90	0.23	53.72	−62.50	13.50
G323.7407−0.2635−MM1	232.9406	−56.5141	−49.53	2.77	157.05	2.80	1.81	3114.39	−50.50	17.00
G326.4745+0.7027−MM1	235.8187	−54.1205	−40.20	3.41	149.75	2.50	0.77	122.27	−38.50	14.00
G326.6411+0.6127−MM1	236.1381	−54.0912	−43.55	1.85	108.45	2.50	4.37	30.79	−42.60	10.50
G328.2353−0.5481−MM1	239.4916	−53.9899	−40.23	1.99	94.10	2.50	1.10	1340.24	−44.70	15.50
G328.2551−0.5321−MM1	239.5009	−53.9668	−43.12	2.40	93.70	2.50	0.49	360.81	−37.50	15.00
G328.8087+0.6328−MM1	238.9530	−52.7182	−41.28	3.45	269.83	2.50	1.30	351.70	−44.40	1.00
G328.8087+0.6328−MM3	238.9513	−52.7164	−41.28	0.83	22.37	2.50	3.18	300.00	−44.00	5.50
G329.0303−0.2022−MM1	240.1333	−53.2076	−38.79	1.80	66.38	2.50	0.22	26.00	−45.80	7.00
G329.0303−0.2022−MM2	240.1295	−53.2137	−38.79	1.76	70.86	2.50	0.26	118.00	−37.10	8.00
G329.1835−0.3147−MM1	240.4476	−53.1954	−49.07	2.19	251.79	4.20	0.29	5.14	−55.60	10.00
G332.9630−0.6781−MM1	245.3450	−50.8830	−42.48	1.37	172.85	4.20	0.61	26.00	−45.90	16.00
G333.1298−0.5602−MM3	245.3991	−50.6809	−56.42	0.57	59.80	4.20	0.35	25.50	−56.80	8.00
G333.1298−0.5602−MM2	245.3978	−50.6824	−56.42	0.73	82.42	4.20	0.59	9.00	−52.70	9.00
G333.2332−0.0606−MM1	244.9622	−50.2529	−87.45	1.78	1327.85	10.30	1.13	0.70	−85.30	5.00
G333.2332−0.0606−MM2	244.9622	−50.2529	−87.45	1.36	838.01	10.30	0.73	1.30	−91.90	12.50
G333.4659−0.1641−MM1	245.3342	−50.1629	−42.48	2.26	255.59	4.20	2.20	30.00	−42.30	12.00
G335.5857−0.2906−MM1	247.7250	−48.7316	−46.22	4.53	403.36	3.80	0.29	29.00	−47.30	3.00
G335.7896+0.1737−MM1	247.4501	−48.2645	−49.46	2.05	208.45	3.80	0.71	170.00	−47.50	14.00
G336.0177−0.8283−MM1	248.7839	−48.7800	−47.41	2.73	353.15	3.80	0.89	90.00	−53.10	15.50
G337.7045−0.0535−MM1	249.6231	−47.0100	−46.52	4.75	3876.34	12.50	0.42	171.00	−54.60	9.00
G337.7045−0.0535−MM3	249.6239	−47.0113	−46.52	1.19	751.27	12.50	0.86	13.00	−44.00	9.00
G338.0748+0.0111−MM1	249.9118	−46.6923	−39.67	0.98	1367.35	12.80	1.27	3.60	−41.60	12.50
G338.0748+0.0111−MM2	249.9141	−46.6912	−39.67	0.95	1065.81	12.80	0.26	13.40	−43.90	11.00
G338.9249+0.5539−MM2	250.1558	−45.6936	−64.09	1.38	197.56	3.90	0.15	8.00	−65.60	7.00
G338.9266+0.6329−MM1	250.0687	−45.6415	−61.63	1.21	135.19	3.90	0.24	3.80	−64.50	9.00
G338.9266+0.6329−MM2	250.0817	−45.6426	−61.63	0.69	70.76	3.90	0.21	64.00	−61.30	10.00
G339.6802−1.2090−MM2	252.7772	−46.2675	−27.95	0.69	13.39	1.80	0.16	72.00	−21.40	19.50
G339.6802−1.2090−MM3	252.7772	−46.2661	−27.95	0.55	11.77	1.80	0.22	23.00	−34.40	2.00
G340.9698−1.0212−MM1	253.7407	−45.1513	−23.94	2.22	49.95	1.80	1.44	10.20	−31.40	15.00
G343.7559−0.1640−MM1	255.1864	−42.4359	−26.91	5.26	93.53	1.80	1.12	5.20	−30.70	8.50
G344.2275−0.5688−MM1	256.0362	−42.3109	−22.03	7.54	155.15	2.00	0.80	91.00	−19.80	19.50
G348.5493−0.9789−MM1	259.8358	−39.0643	−15.45	1.50	41.80	1.80	0.22	41.10	−10.60	12.00
G349.0915+0.1059−MM1	259.1024	−37.9961	−77.56	2.13	1852.21	11.00	0.42	9.90	−81.50	5.00
G351.4441+0.6579−MM3	260.2280	−35.7521	−3.91	2.03	31.63	1.70	2.60	129.00	−7.00	15.00
G351.5815−0.3528−MM1	261.3572	−36.2124	−96.69	6.20	2028.80	5.80	2.16	47.50	−94.20	12.00
G351.7747−0.5369−MM1	261.6541	−36.1550	−2.00	13.92	108.95	1.00	0.98	231.00	1.30	12.00
G357.9667−0.1626−MM1	265.3347	−30.7519	−2.89	5.32	622.04	5.00	0.57	47.50	−3.10	6.00
G354.6154+0.4719−MM1	262.5722	−33.2319	−2.72	3.63	69.86	1.70	0.40	166.00	−24.40	14.50
G358.4601−0.3924−MM1	265.8612	−30.4535	−2.50	0.99	218.09	5.00	1.46	47.73	−1.30	4.50
G358.4601−0.3924−MM2	265.8644	−30.4543	−2.50	0.42	81.92	5.00	1.44	11.19	−7.30	14.50

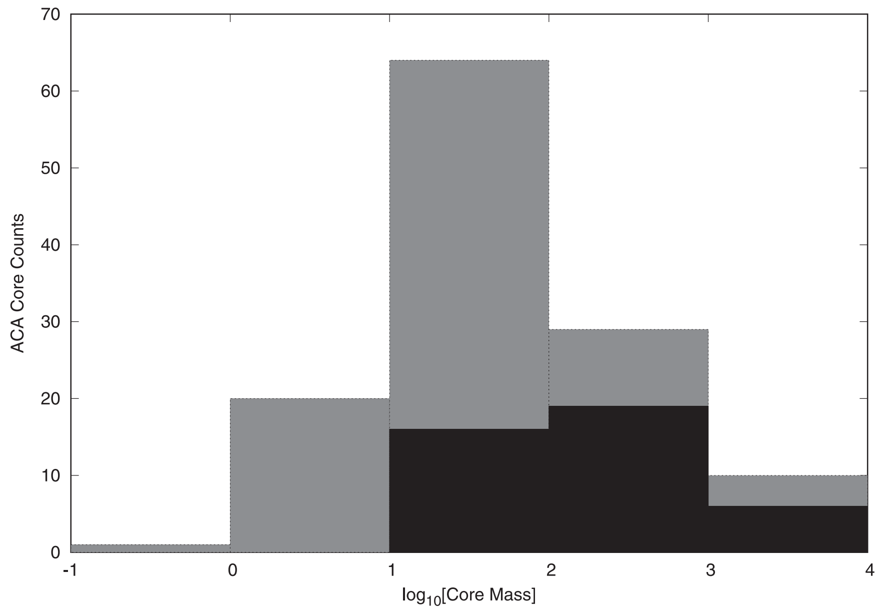

Figure 4. Comparative smoothened mass distribution of all the ACA cores/clumps with 10 $M_{\odot}$ binning. The gray and black bars indicate all cores and 6.7 GHz CH_3OH maser-associated cores, respectively.

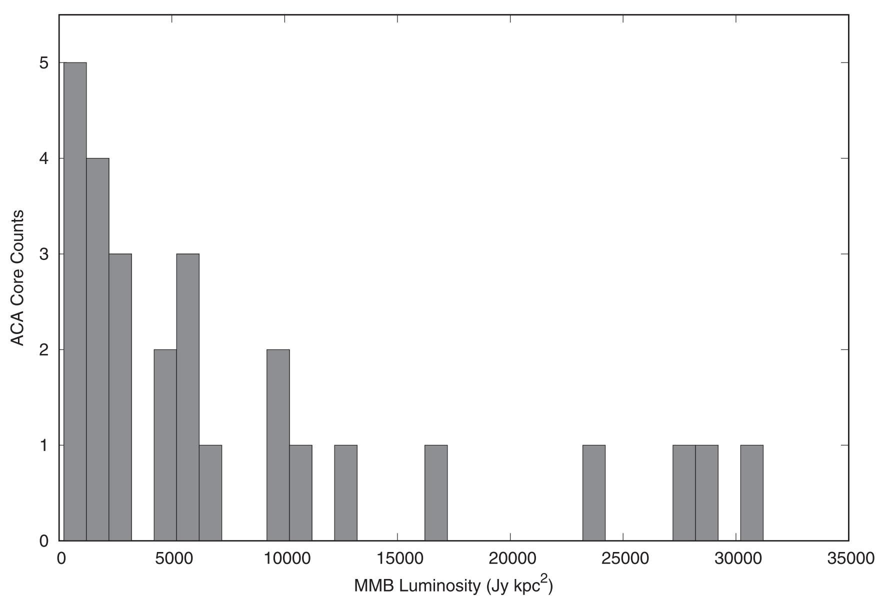

Figure 5. Plot of MMB luminosity distribution of the ACA-MMB with a binning of 1000 Jy kpc^2.

component(s) of 6.7 GHz CH_3OH masers. We found 42 of the 112 ACA cores to be associated with 6.7 GHz CH_3OH masers. The details of the cores associated with the masers are shown in Table 1. This represents 37.5% of the cores, and may be affected by the flux limits of the MMB survey, and mass bias since 6.7 GHz CH_3OH masers are known to be exclusively associated with already formed high-mass protostars. The lowest mass core with CH_3OH maser association is $\sim$12 $M_{\odot}$. The figures in the Appendix show ACA 870 μm line-free continuum emissions with the positions of the ATLASGAL continuum peaks, class I 44/95 GHz CH_3OH masers, class II 6.7 GHz CH_3OH masers, and 22 GHz H_2O masers indicated by stars, diamonds, circles, and triangles, respectively.

Applying the criteria outlined in Section 3, we narrowed the number of cores used in our statistical considerations to 27 cores. We have used the term *unflagged ACA-MMB* to describe cases where all 42 ACA-MMB sources were used without applying the criteria in Section 3.

4.1. ACA-MMB Core Angular Offsets

The angular offsets of the ACA cores from the 6.7 GHz CH_3OH maser peak positions range from $0\farcs15$ to $4\farcs37$. Figure 1 shows a histogram of the surface density of 6.7 GHz CH_3OH masers as a function of the angular separation between the maser peaks and the ACA core peaks. We derived the mean offsets to be $0\farcs92 \pm 0\farcs20$.

Comparing Figure 1 with its clump scale equivalent in Urquhart et al. (2013), we find a drop in the maser angular surface density of the 6.7 GHz CH_3OH masers at angular separations larger than $1''$. This implies that MMB associations

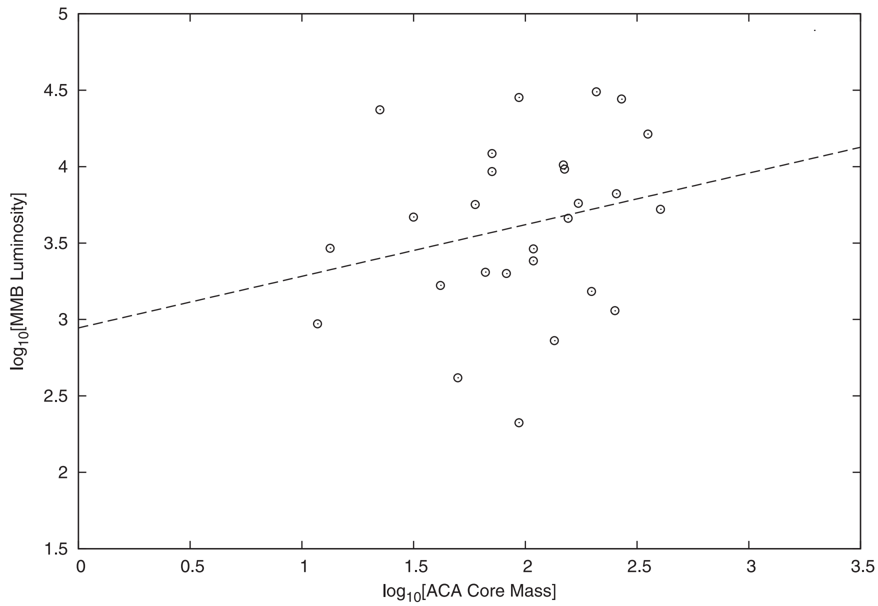

Figure 6. Linear relation between the MMB luminosities and the ACA core masses, with a correlation coefficient of 0.24.

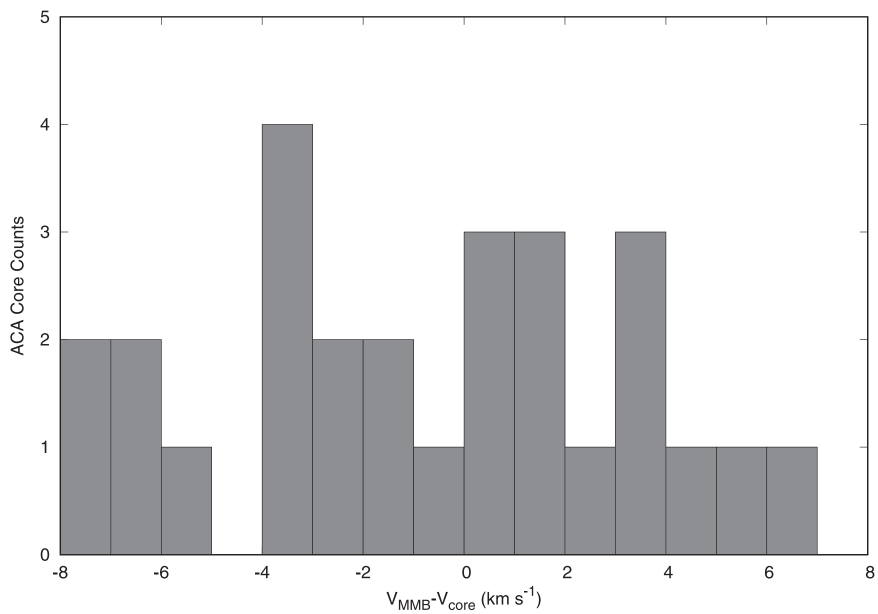

Figure 7. Distribution of the differences between the systemic velocities of the ACA cores and their peak velocities of their associated MMB 6.7 GHz CH_3OH masers.

with the massive dense cores (MDCs) are more robust than those reported by Urquhart et al. (2013).

4.2. ATLASGAL and ACA-MMB Flux Densities

In this subsection, we consider the *unflagged ACA-MMB* in our consideration. Figure 2 shows the plot of the ATLASGAL dust continuum peak flux densities against those of their associated ACA dust continuum emissions. We have checked the correlation of the ATLASGAL dust continuum flux densities with the 0.9 mm continuum flux densities of their ACA counterpart. We obtained a good correlation coefficient of 0.56 with a significance value of 2×10^{-10}, presenting the expected correlation of flux densities from clump-to-core scales. It should be noted that all the correlation coefficients reported in this work were derived from linear regression analysis.

However, we obtained a weak correlation of coefficient 0.29 between the ACA peak flux densities and the MMB peak fluxes. This is a 0.1 improvement from the results of Urquhart et al. (2013), though they had a better significance value considering that their sample size is an order of magnitude larger than ours. The improvement in the correlation could be an indicator of core-scale-to-maser-intensity relation. Figure 3 shows the MMB-ACA peak flux distribution in logarithm scale.

5. Discussion

5.1. ACA-MMB Mass Distribution

Adopting the core masses of Csengeri et al. (2017) derived with dust temperature of 25 K, we compared the mass distribution of ACA cores with 6.7 GHz CH_3OH masers (ACA-MMB). The mass range of the *unflagged ACA-MMB* is 11.8–3876.3 $M_{\odot}$, while for the more constrained sample of 27 cores the range is 11.8–403.4 $M_{\odot}$.

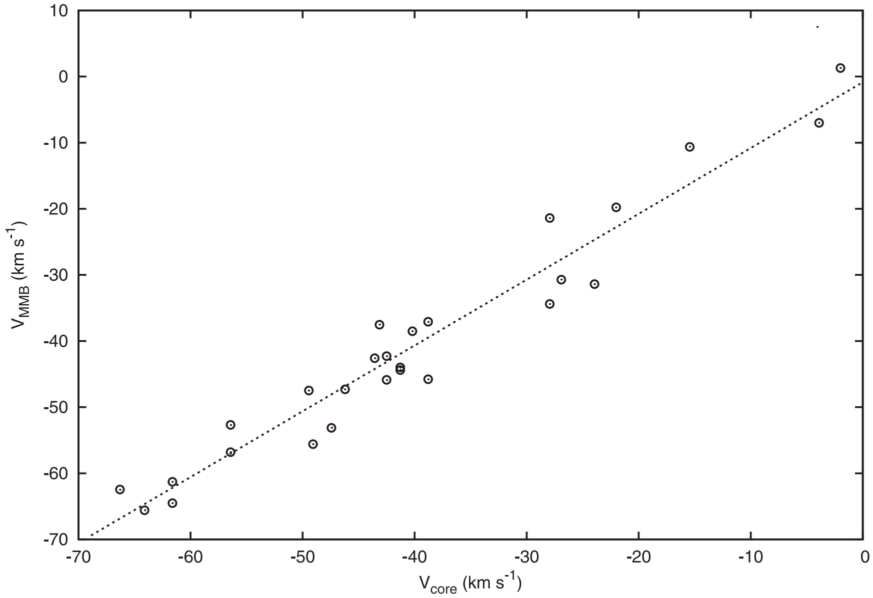

Figure 8. MMB V_{LSR} against core V_{LSR} plot.

Figure 4 shows the distribution of the core masses of the ACA-MMB (black bars) compared with those without 6.7 GHz CH_3OH masers. The average mass of the ACA-MMB was obtained to be 134.3 ± 19.3 $M_\odot$.

5.2. MMB Luminosity–Core Mass Relation

Using the derived kinematic distances, D, of the cores and the peak flux densities, S_ν, of the 6.7 GHz CH_3OH masers with the assumption of isotropic maser emission, we calculated the luminosities ($4\pi D^2 S_\nu$) of the MMBs. Figure 5 shows the distribution of maser luminosities of the ACA-MMBs.

We have also compared the linear relationship between the MMB luminosities and their associated ACA core masses. Figure 6 shows the plot of MMB luminosities against ACA core masses in logarithm scale. We found the linear relation to be $\log_{10}$(MMB luminosity) = $(0.338 \pm 0.275)\log_{10}$(ACA core mass) $+(2.945 \pm 0.555)$. There is a weak correlation coefficient of 0.24 between them.

5.3. Core and MMB Local Standard of Rest Velocities

Statistically, we have compared the systemic velocities of the ACA cores with the V_{LSR} of the MMB 6.7 GHz CH_3OH maser peaks. Figure 7 shows the distribution of the real values of the difference in V_{LSR} of the MMB and the ACA cores (derived from the ALMA molecular line). We found approximately 50%–50% distribution in the -8 to 0 km s^{-1} and 0 to 8 km s^{-1} sides.

Figure 8 shows the scatter plot of the V_{LSR} of the MMB against the V_{LSR} of the ACA cores. We found a strong correlation, of coefficient 0.97, between them. The dotted lines shows the best linear fit of the relation, $V_{MMB} = (1.002 \pm 0.048) V_{core} - (0.578 \pm 2.074)$.

5.4. Earliest Stage Trapezium

In Figure 2, we showed a skewed square representing the ACA weak-continuum containing about 45 ACA cores without CH_3OH masers. The enclosed cores show no association with MMB 6.7 GHz CH_3OH masers. We confirmed that the search for the masers covered the location of the cores, with no detections. The non-detection of the class II masers is an indication that the cores within the trapezium are at a much earlier phase of their protostellar evolution. The clump-to-core flux relation within the enclosed portion could form the basis for identifying cores within known clumps at the earliest evolutionary stage. These objects are already driving outflows but do not have enough radiative power to pump 6.7 GHz CH_3OH masers.

6. Conclusions and Summary

We have compared the positional correlation of MDC identified with ACA and class II CH_3OH masers of the MMB survey and found a 37.5% maser association rate with the mass of the least massive core (with maser) being ∼12 $M_\odot$. Ninety percent of the MDC associated with 6.7 GHz CH_3OH masers have masses >40 $M_\odot$.

Our statistical analysis of the maser-associated MDCs is more robust because we have smaller positional offsets between the core peaks and the masers (ranges from 0″.17 to 4″.79). We obtained a weak correlation between the peak fluxes of the 0.9 mm continuum cores and their associated 6.7 GHz CH_3OH masers.

This paper makes use of the following ALMA data: [ADS/JAO.ALMA#2013.1.00960.S]. ALMA is a partnership of ESO (representing its member states), NSF (USA), and NINS (Japan), together with NRC (Canada), NSC, and ASIAA (Taiwan), and KASI (Republic of Korea), in cooperation with the Republic of Chile. The Joint ALMA Observatory is operated by ESO, AUI/NRAO, and NAOJ. Part of the data are retrieved from the JVO portal (http://jvo.nao.ac.jp/portal) operated by the NAOJ. T.C. acknowledges support from the *Deutsche Forschungsgemeinschaft,* DFG, via the SPP (priority programme) 1573 “Physics of the ISM.”

Appendix
Spatial Position of CH_3OH and H_2O Masers Associated with the ALMA Cores/Clumps

Having matched all the ALMA cores with the available 6.7 GHz CH_3OH and ∼22 GHz H_2O masers, we here provide the images showing the spatial positions of the masers relative to the ALMA core. 6.7 GHz CH_3OH and ∼22 GHz H_2O masers are represented by open circles and triangles, respectively.

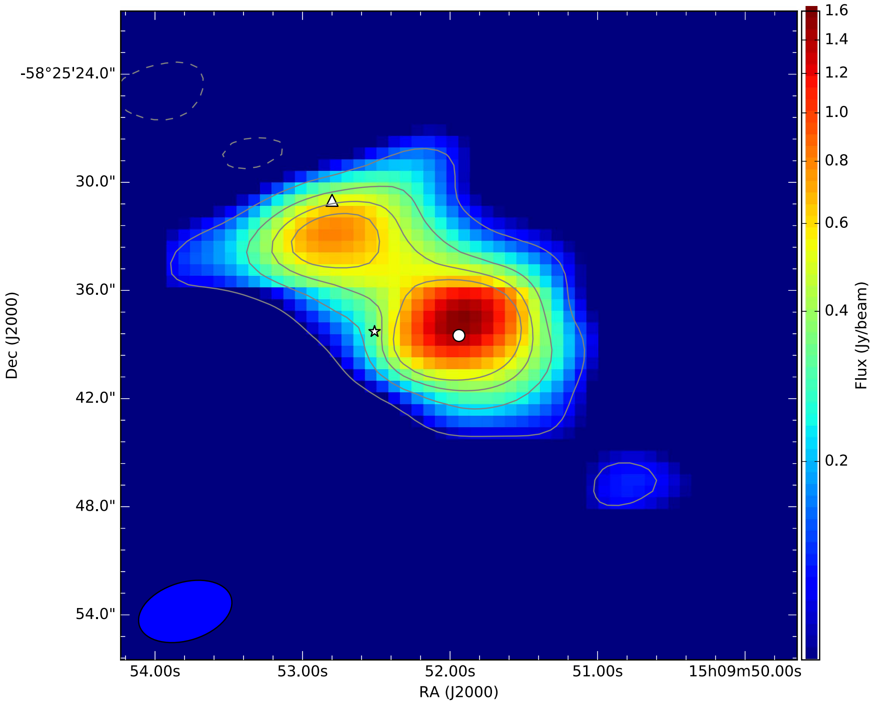

Figure 9. G320.2325. The white filled star, circle, triangle, and diamond with black edges represent the peak position of ATLASGAL clumps, 6.7 GHz CH_3OH masers, H_2O masers, and 44 GHz CH_3OH masers, respectively. A filled diamond with blue edge color indicates class I 95 GHz CH_3OH masers. These symbols are the same for the rest of the figures of the ACA cores.

(The complete figure set (46 images) is available.)

References

Bartkiewicz, A., Szymczak, M., van Langevelde, H. J., Richards, A. M. S., & Pihlström, Y. M. 2009, A&A, 502, 155
Bayandina, O. S., Val'tts, I. E., & Larionov, G. M. 2012, ARep, 56, 553
Breen, S. L., Ellingsen, S. P., Caswell, J. L., et al. 2011, ApJ, 733, 80
Breen, S. L., Ellingsen, S. P., Caswell, J. L., & Lewis, B. E. 2010, MNRAS, 401, 2219
Breen, S. L., Ellingsen, S. P., Contreras, Y., et al. 2013, MNRAS, 435, 524
Caswell, J. L., Fuller, G. A., Green, J. A., et al. 2010, MNRAS, 404, 1029
Caswell, J. L., Fuller, G. A., Green, J. A., et al. 2011, MNRAS, 417, 1964
Chibueze, J. O., Imai, H., Tafoya, D., et al. 2012, ApJ, 748, 146
Chibueze, J. O., Omodaka, T., Handa, T., et al. 2014, ApJ, 784, 114
Codella, C., Lorenzani, A., Gallego, A. T., Cesaroni, R., & Moscadelli, L. 2004, A&A, 417, 615
Contreras, Y., Schuller, F., Urquhart, J. S., et al. 2013, A&A, 549, A45
Cragg, D. M., Johns, K. P., Godfrey, P. D., & Brown, R. D. 1992, MNRAS, 259, 203
Cragg, D. M., Sobolev, A. M., & Godfrey, P. D. 2005, MNRAS, 360, 533
Csengeri, T., Urquhart, J. S., Schuller, F., et al. 2014, A&A, 565, A75
Csengeri, T., Bontemps, S., Wyrowski, F., et al. 2017, A&A, in press
Cyganowski, C. J., Brogan, C. L., Hunter, T. R., & Churchwell, E. 2009, ApJ, 702, 1615
De Buizer, J. M. 2003, MNRAS, 341, 277
de Villiers, H. M., Chrysostomou, A., Thompson, M. A., et al. 2015, MNRAS, 449, 119
Fujisawa, K., Aoki, N., Nagadomi, Y., et al. 2014, PASJ, 66, 109
Gerner, T., Beuther, H., Semenov, D., et al. 2014, A&A, 563, A97
Green, J. A., Caswell, J. L., Fuller, G. A., et al. 2012, MNRAS, 420, 3108
Higuchi, A. E., Hasegawa, T., Saigo, K., Sanhueza, P., & Chibueze, J. O. 2015, ApJ, 815, 106
Ilee, J. D., Cyganowski, C. J., Nazari, P., et al. 2016, arXiv:1608.05561
Kalenskii, S. V., Johansson, L. E. B., Bergman, P., et al. 2010, MNRAS, 405, 613
Matsumoto, N., Hirota, T., Sugiyama, K., et al. 2014, ApJL, 789, L1
Menten, K. 1991, in Atoms, Ions and Molecules: New Results in Spectral Line Astrophysics 16, 119
Minier, V., Ellingsen, S. P., Norris, R. P., & Booth, R. S. 2003, A&A, 403, 1095
Plambeck, R. L., & Menten, K. M. 1990, ApJ, 364, 55
Reid, M. J. 2007, in Astrophysical Masers and their Environments 242, 522
Sánchez-Monge, Á., Cesaroni, R., Beltrán, M. T., et al. 2013, A&A, 552 L10
Schuller, F., Menten, K. M., Contreras, Y., et al. 2009, A&A, 504, 415
Sobolev, A. M., & Deguchi, S. 1994, A&A, 291, 569
Urquhart, J. S., Moore, T. J. T., Schuller, F., et al. 2013a, MNRAS, 431 1752
Urquhart, J. S., Thompson, M. A., Moore, T. J. T., et al. 2013b, MNRAS, 435, 400
Walsh, A. J., Breen, S. L., Britton, T., et al. 2011, MNRAS, 416, 1764
Xu, Y., Li, J. J., Hachisuka, K., et al. 2008, A&A, 485, 729